Supporting Information: Designed Post-Self-Assembly Structural and Functional Modifications of a Truncated Tetrahedron

Yao-Rong Zheng, Wen-Jie Lan, Ming Wang, Timothy R. Cook, and Peter J. Stang**

Department of Chemistry, University of Utah, 315 South 1400 East, RM 2020, Salt Lake City, Utah, 84112

E-mail: stang@chem.utah.edu, zhengyaorong@gmail.com

Table of Content

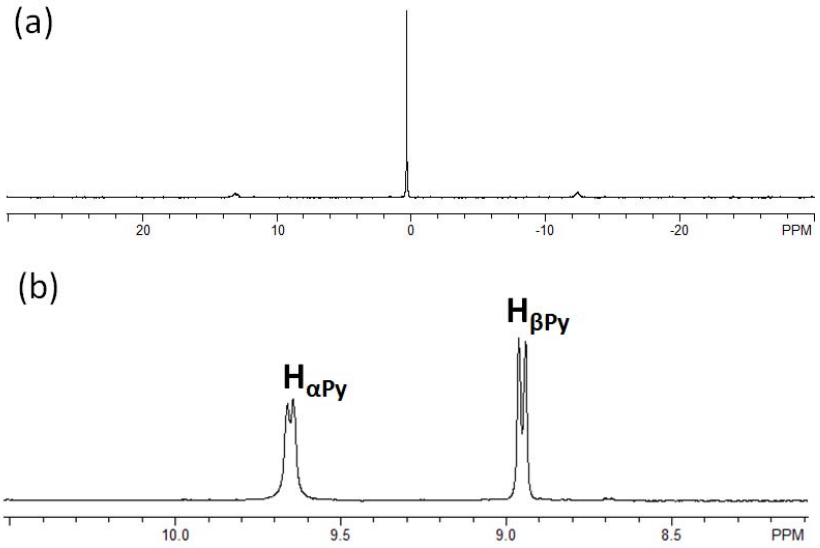

Figure S1. (a) $^{31}P\{^{1}H\}$ and (b) Partial ^{1}H NMR (Acetone-d_6, 300MHz) spectrum of the [6 + 4] metal-organic supramolecule **3**.

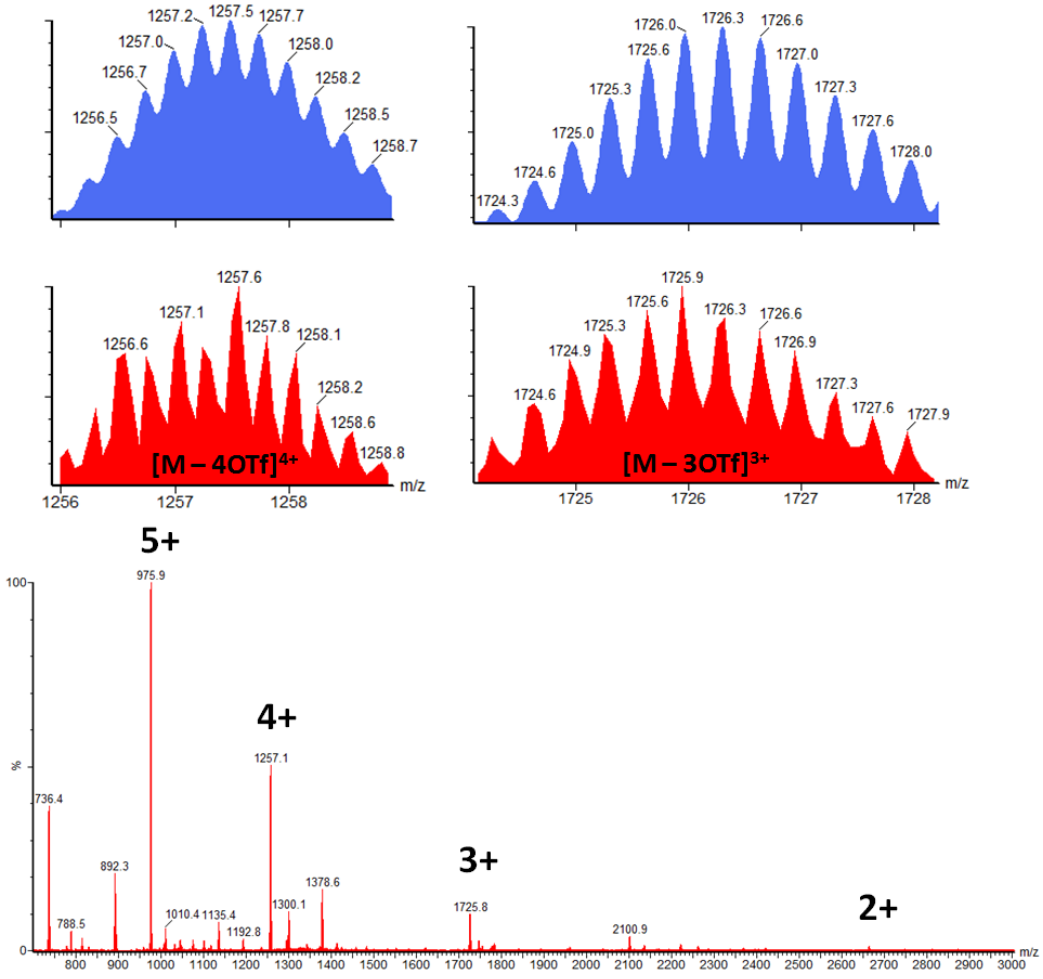

Figure S2. Full ESI MS spectrum of the [6 + 4] metal-organic supramolecule **3**.

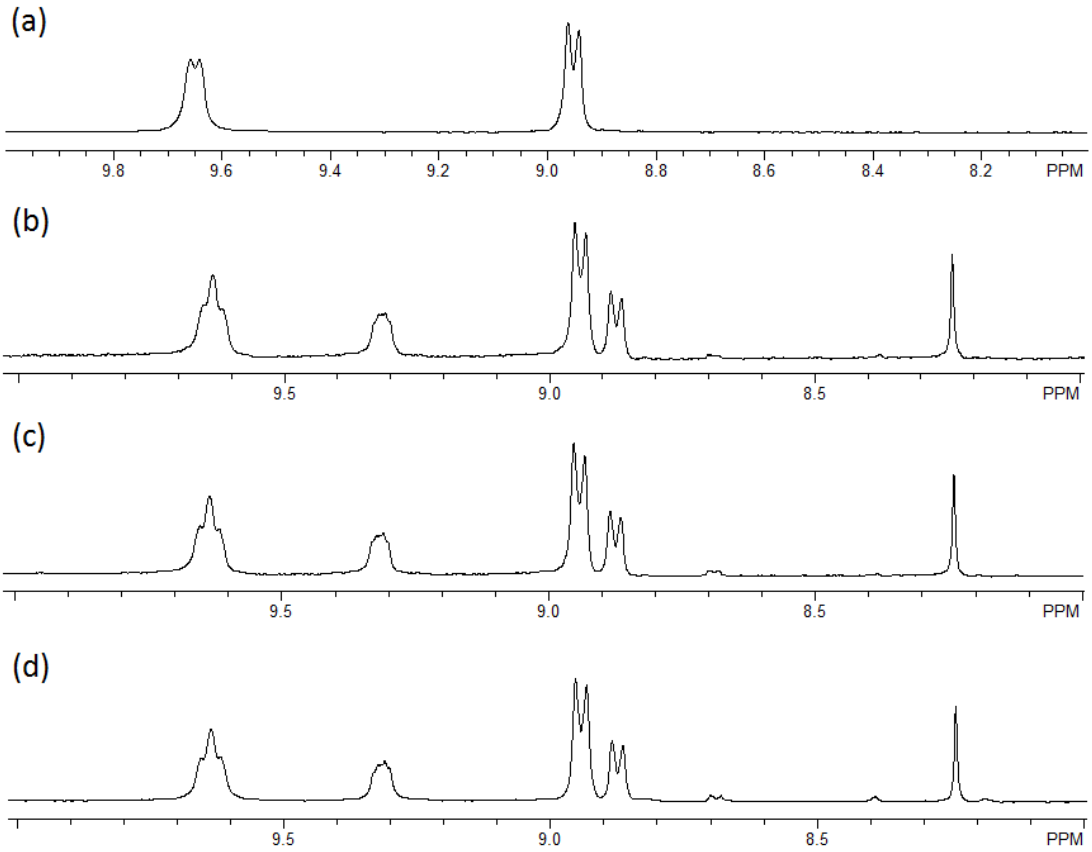

Figure S3. (a) ^{1}H NMR spectrum (Acetone-d_6, 300 MHz) of the discrete [6 + 4] metal-organic supramolecule (**3**); (b and c) ^{1}H NMR spectra of component substitution of **3** to **5**; (d) ^{1}H NMR spectrum of self-assembly of **5** by individual molecular components.

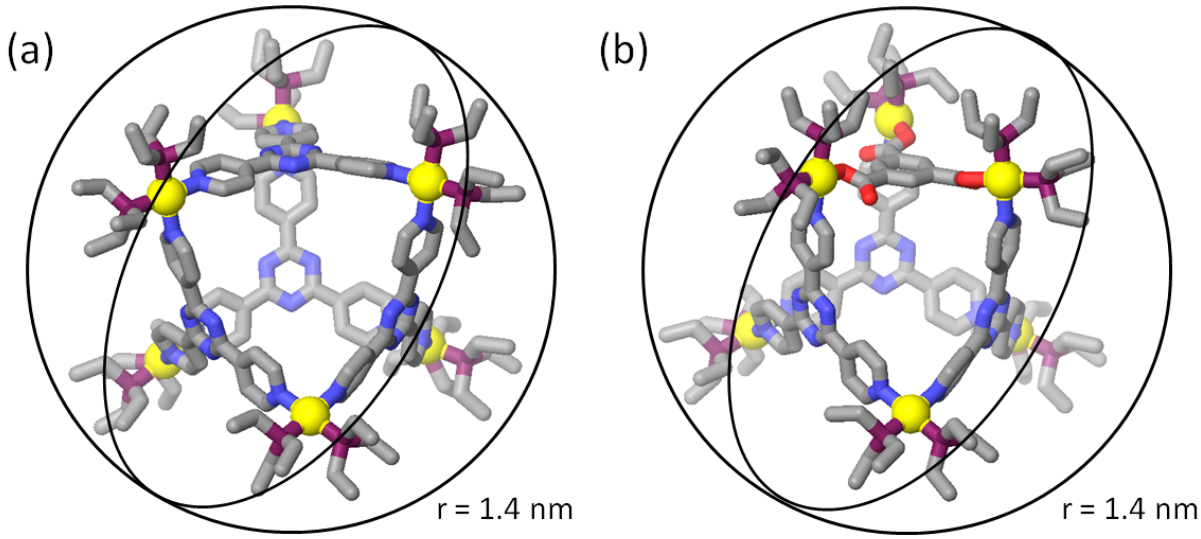

Figure S4. MMFF models of (a) the discrete [6 + 4] metal-organic supramolecule **3** and (b) the three-component modified supramolecule **5**.

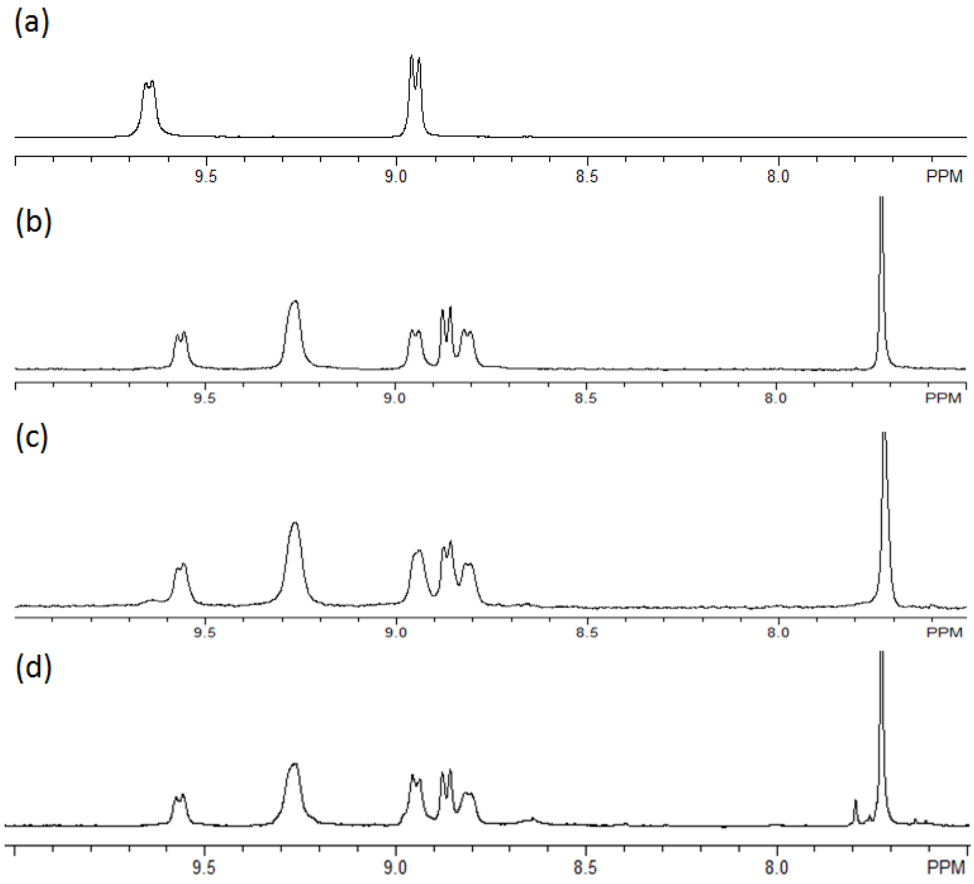

Figure S5. (a) ^{1}H NMR spectrum of the discrete [6+4] metal-organic supramolecule **3**; (b and c) ^{1}H NMR spectra of component substitution of **3** to **7**; (d) ^{1}H NMR spectrum of self-assembly of **7** by individual molecular components.

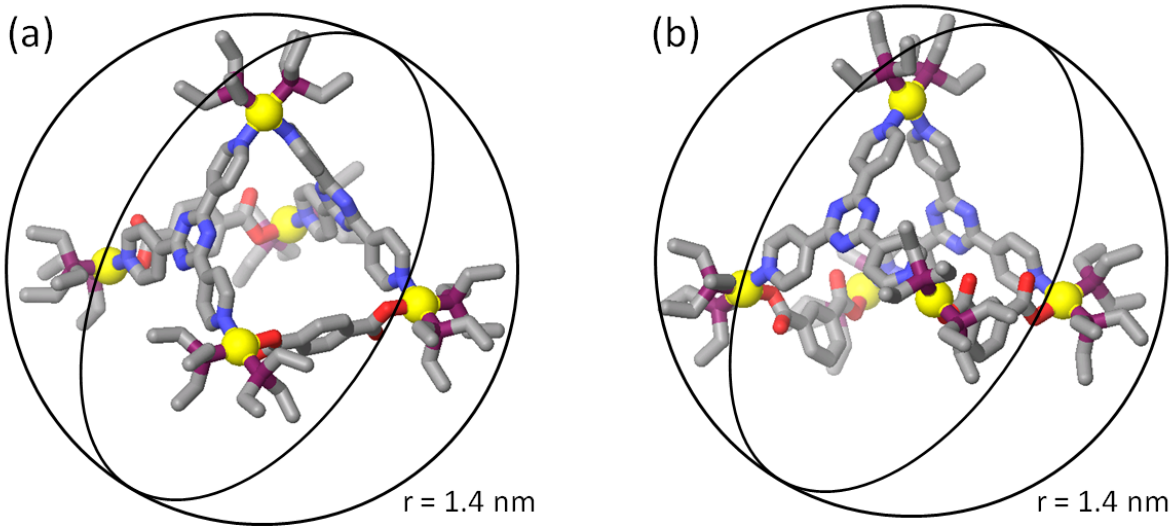

Figure S6. MMFF models of (a) the structurally modified supramolecule **7** and (b) the non-functional scaffold **9**.

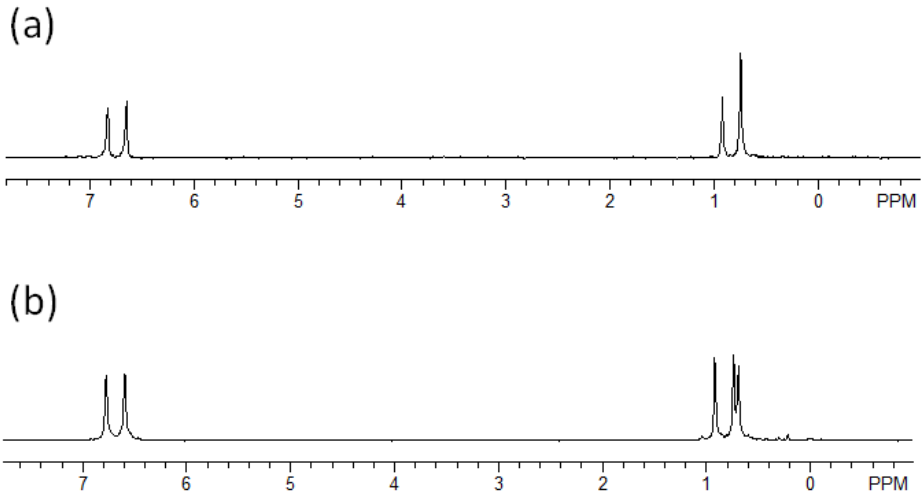

Figure S7. $^{31}P\{^{1}H\}$ NMR (Acetone-d_6, 300MHz) spectra of the non-functional scaffold **9** (a) and the ferrocenyl functionalized supramolecule **11** (b).

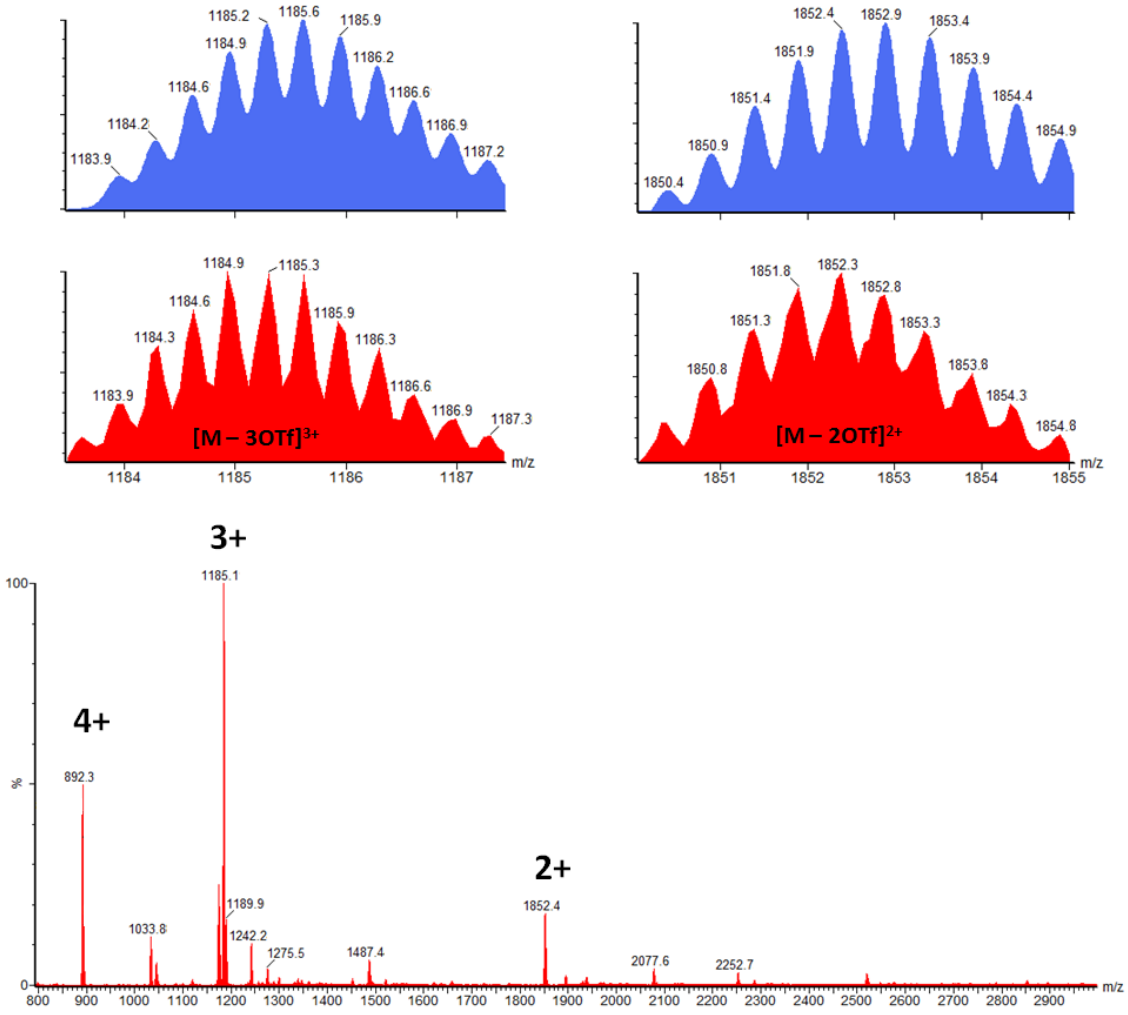

Figure S8. Full ESI-MS spectrum of the triflate salt of non-functional scaffold **9**.

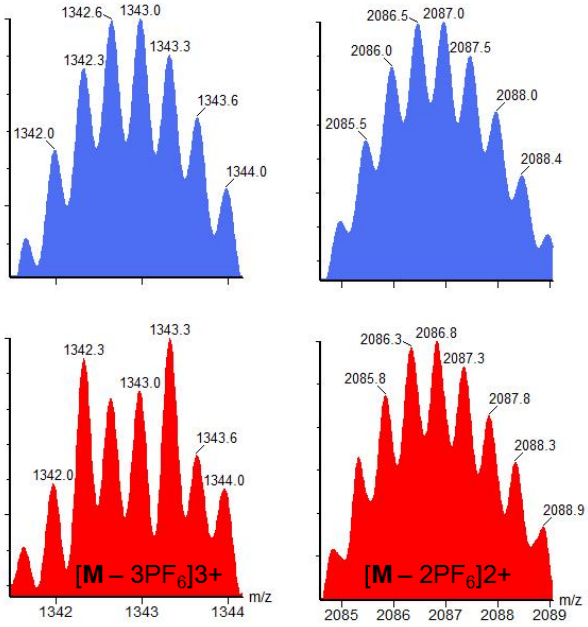

Figure S9. Calculated (top, blue) and experimental (bottom, red) isotopically resolved ESI-MS spectra of the PF_6 salt of ferrocenyl functionalized supramolecule **11**.

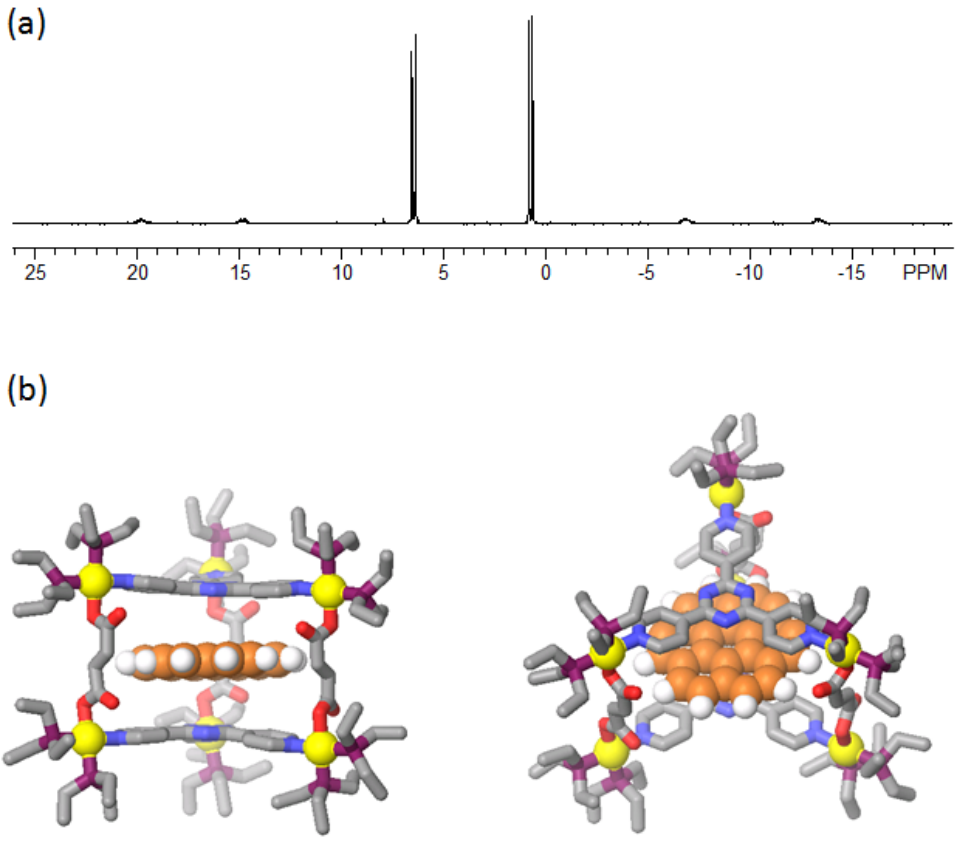

Figure S10. (a) $^{31}P\{^{1}H\}$ NMR (Acetone-d_6, 300MHz) spectrum of the host-guest complex **13** and (b) different views of the MMFF model of **13**.

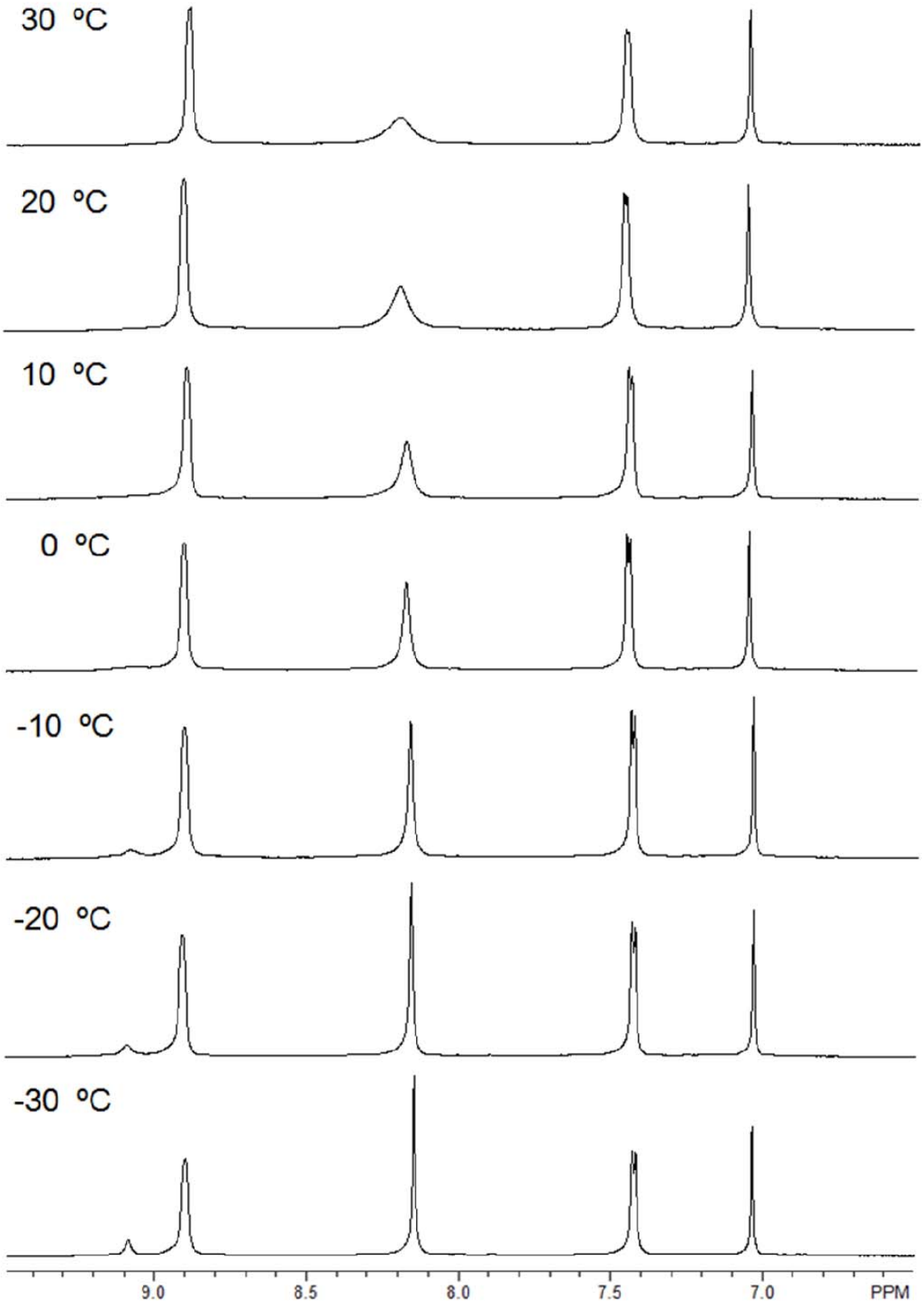

Figure S11. Variable temperature ^{1}H NMR (Acetone-d_6, 500MHz) spectra of the host-guest complex **13**.

Experimental details for the Pulsed Field Gradient Spin Echo (PGSE) NMR measurements

Pulsed gradient spin-echo (PGSE) NMR diffusion measurements were done by pulse-sequence method developed by Stejskal and Tanner:

$$\mathrm{In}(I/I_0) = \gamma_x^2\delta^2G^2(\Delta - \delta/3)D$$

γ_x : Gyromagnetic ratio of the x-nucleus

δ: Length of the gradient pulse

G: Gradient strength

Δ: Delay between the midpoints of gradients

D: Diffusion coefficient

Temp: 298K

Instrument: Inova 500 MHz

Stokes-Einstein Equation: The molecular size is obtained from the diffusion coefficient via the Stokes-Einstein equation shown below:

$$D = k_BT/6\pi\eta r$$

k_B: Boltzmann constant

T: Absolute temperature

r: Hydrodynamic radius of the species under investigation

D: Diffusion coefficient

Gradient Calibration: The gradient strengths need to be carefully calibrated to obtain accurate D values to fit equation (1). Gradient strengths were calibrated using the width (in Hz) of a sample of known length along the NMR-tube (Z) axis, back-calculation of the coil constant from a diffusion experiment on D_2O using $D = 1.9 \times 10^{-5}$ cm^2/s for D_2O at 298K was used to calculate the gradient strengths of both the probes.

D(**3**) = (5.37 ± 0.13) x 10^{-6} cm^2/s; D(**5**) = (5.42 ± 0.16) x 10^{-6} cm^2/s;

D(**7**) = (5.46 ± 0.12) x 10^{-6} cm^2/s; D(**9**) = (5.25 ± 0.09) x 10^{-6} cm^2/s;

D(**11**) = (4.38 ± 0.18) x 10^{-6} cm^2/s; D(**13**) = (5.50 ± 0.18) x $10^{-6}$$cm^2/s$.

Electrochemistry analysis of **3**, **9**, and **11**

All electrochemical measurements were performed in a Faraday cage using a Pine Instrument Co. RDE3 potentiostat/waveform generator, or using a Dagan Cornerstone Chem-Clamp potentiostat combined with the RDE3 waveform generator. These instruments were interfaced to a computer through a PCI 6251 data acquisition board (National Instruments). Voltammetric curves and current-time data were recorded using in-house virtual instrumentation written in LabVIEW 8.0 (National Instruments).

(a) Cyclic voltammetry

The working electrode was a 0.3 mm diameter Pt disk shrouded in glass. A Ag/AgCl and Pt mesh electrode were used as the reference electrode and auxiliary electrode, respectively. Voltammetric experiments on **3** and **9**, Figure S12, show that these molecules are not electrochemically active in acetone within the voltage range examined.

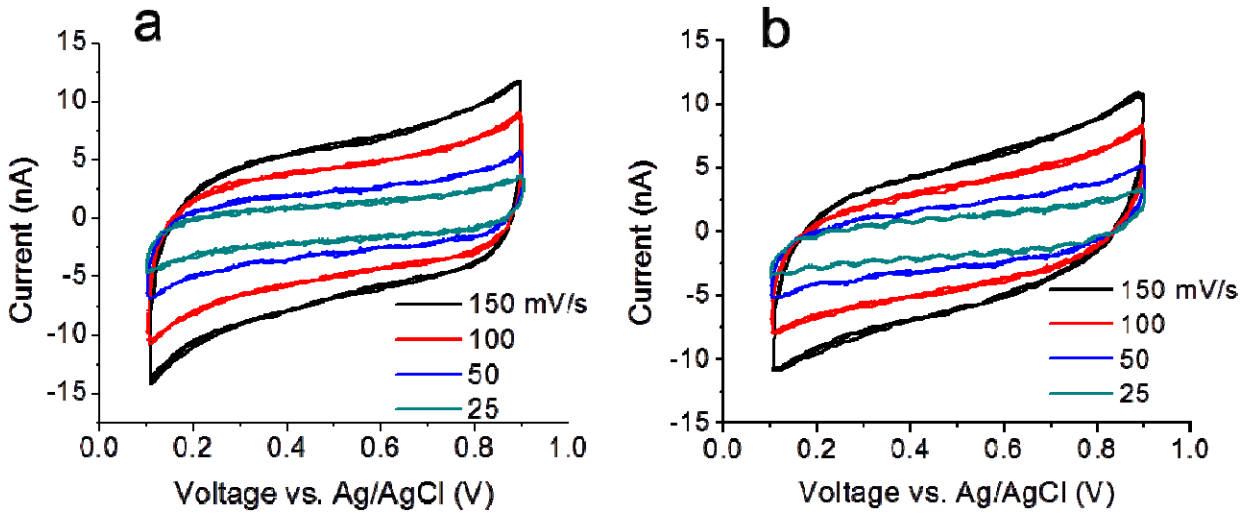

Figure S12. Cyclic voltammetry of (a) **3** and (b) **9** at different scan rates (25-150 mV/s) at a ~0.3 mm diameter Pt electrode. Solution: 0.61 mM **3** and 0.60 mM **9** in acetone containing 0.1 M *n*-Bu_4NPF_6, respectively.

(b) Steady-state electrochemical measurements

Two-electrode steady-state voltammetric measurements of **11** (0.61 mM) in acetone containing 0.1 M *n*-Bu_4NPF_6 were performed using a ~25 μm diameter Pt microdisk electrode as the working electrode and a Ag/AgCl electrode as the combined auxiliary/reference electrode. The radius of the Pt microdisk was provided by the Pt wire manufacturer and further verified from the voltammetric limiting current (i_{lim} = $4nFDca$) for the oxidation of ferrocene. The limiting current for supramolecule is given by:[1]

$$i_{\lim} = 4nFDca\theta_{sites} \quad \text{(SI1)}$$

where n is the number of electrons transferred per ferrocene (= 1), F is Faraday's constant, D is the diffusion coefficient of the supramolecule, c is the molecule bulk concentration, a is the electrode radius, and θ_{sites} is the number of ferrocenyl sites per molecule, respectively. A plot of E vs $\log[(i_{\lim}-i)/i]$ from the steady-state i-V curves (Figure S13) was used to determine if the oxidation of **11** proceeds by independent serial oxidation of the ferrocenyl sites. The slope of this plot was measured to be -0.0678 V, slightly larger than the theoretical expectation of -0.059 V for oxidation of noninteracting ferrocenyl sites, indicating that the redox species almost react independently of one another.

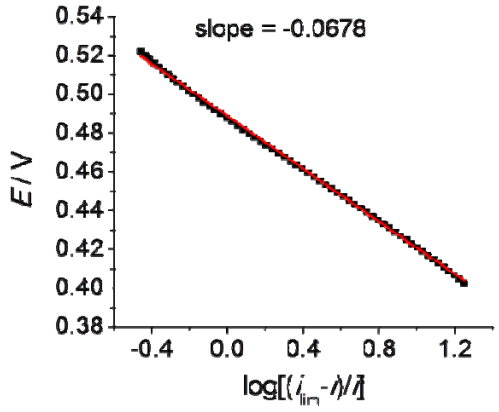

Figure S13. Plot of E vs. $\log[(i_{\lim}-i)/i]$ from the steady-state voltammetric response.

(c) Chronoamperometry measurements

Chronoamperometry measurements were performed to measure the diffusion coefficient of **11**. The potential was stepped from a nonreaction potential to a diffusion-controlled potential, and the resulting time-dependent current (i_t) was monitored. The time-dependent current is given by[2]:

$$\frac{i_t}{i_{\text{lim}}} = 1 + \frac{2}{\pi^{1.5}} a(Dt)^{-0.5} \quad \text{(SI2)}$$

The slope of a plot of i_t/i_{lim} vs $t^{-0.5}$ yields D. This method has been previously used to determine values of D for related supramolecules.[3] Figure S14 shows a plot of i_t/i_{lim} vs $t^{-0.5}$ for the oxidation of **11**, yielding D (eq SI2) and θ_{sites} (eq SI1).

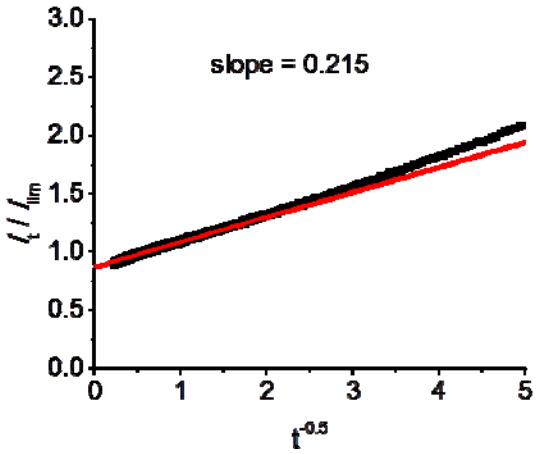

Figure S14. Plot of i_t/i_{lim} vs. $t^{-0.5}$ for the oxidation of **11** in acetone containing 0.1 M *n*-Bu_4NPF_6 using a ~25 μm diameter Pt disk electrode. The black squares are the experimental data and the red line is the fit line in the long-time region.

1. Bard, A. J.; Faulkner, L. R. *Electrochemical Methods: Fundamentals and Applications*; 2nd ed.; John Wiley & Sons: New York, 2001.
2. (a) Denuault, G.; Mirkin, M. V.; Bard, A. J. *J. Electroanal. Chem.* **1991**, *308*, 27. (b) Biondi, C.; Bellugi, L. *J. Electroanal. Chem.* **1970**, *24*, 263. (c) Amatore, C.; Azzali, M.; Calas, P.; Jutand, A.; Lefrou, C.; Rollin, Y. *J. Electroanal. Chem.* **1990**, *288*, 45. (d) Mirkin, M. V.; Nilov, A. P. *J. Electroanal. Chem.* **1990**, *283*, 35. (e) Nowinski, S. A.; Anjo, D. M. *J. Chem. Eng. Data* **1989**, *34*, 265.
3. (a) Ghosh, K.; Hu, J. M.; White, H. S.; Stang, P. J. *J. Am. Chem. Soc.* **2009**, *131*, 6695. (b) Yang, H. B.; Ghosh, K.; Zhao, Y.; Northrop, B. H.; Lyndon, M. M.; Muddiman, D. C.; White, H. S.; Stang, P. J. *J. Am. Chem. Soc.* **2008**, *130*, 839.